Earth and Planetary Science Letters 502 (2018) 46–56

Contents lists available at ScienceDirect

Earth and Planetary Science Letters

www.elsevier.com/locate/epsl

Prospects for an ancient dynamo and modern crustal remanent magnetism on Venus

Joseph G. O'Rourke [a,*], Cédric Gillmann [b,c], Paul Tackley [d]

[a] School of Earth and Space Exploration, Arizona State University, Tempe, AZ, United States of America
[b] Royal Observatory of Belgium, Brussels, Belgium
[c] Free University of Brussels, Department of Geosciences, G-Time, Brussels, Belgium
[d] Department of Earth Sciences, ETH Zurich, Institute of Geophysics, Zurich, Switzerland

ARTICLE INFO

Article history:
Received 29 January 2018
Received in revised form 16 June 2018
Accepted 28 August 2018
Available online xxxx
Editor: B. Buffett

Keywords:
Venus
Venus, interior
Venus, surface
magnetic fields
accretion

ABSTRACT

Venus lacks an internally generated magnetic field today. Whether one existed in the past is unknown, but critical to atmospheric evolution and potential habitability. Canonical models assume the core of Venus is cooling too slowly for convection and thus a magnetic dynamo to occur today. Core/mantle heat flow is suppressed in these models after a putative transition in mantle dynamics associated with widespread, volcanic resurfacing. However, recent studies of impact craters and other surface features support more steady heat loss over geologic time. Precipitation of MgO and/or SiO_2 from the core can also drive compositional convection even with slow cooling. Here we reevaluate the likelihood that Venus has an "Earth-like" (at least partially liquid and chemically homogeneous) core using numerical simulations of the coupled atmosphere–surface–mantle–core evolution. An Earth-like core is only compatible with the modern lack of a dynamo if the thermal conductivity of core material is towards the higher end of modern estimates (i.e., >100 $W\,m^{-1}\,K^{-1}$). If lower estimates like $\sim$40–50 $W\,m^{-1}\,K^{-1}$ are actually correct, then we favor recent proposals that the core has completely solidified or preserved primordial stratification. Any simulation initialized with a homogeneous, liquid core predicts a global magnetic field with Earth-like surface strength for $>$2–3 billion years after accretion—consistent with all available observations—and also sporadic activity within the surface age while temperatures remain below the Curie point of magnetite. Therefore, future spacecraft missions should prioritize the first-ever magnetometer measurements below the ionosphere to search for crustal remanent magnetism.

1. Introduction

Venus stands alone as the only major planet without evidence for an internally generated magnetic field either now or in the past. Vigorous convection of liquid iron alloy in Earth's outer core has sustained our geodynamo for at least 3.45 Gyr (e.g., Tarduno et al., 2010). Venus is presumably differentiated like Earth into a silicate mantle and metallic core, but Pioneer Venus Orbiter constrained the magnetic moment of Venus to less than $\sim 10^{-5}$ times the modern value for Earth (e.g., Phillips and Russell, 1987). Determining whether Venus ever hosted a global magnetic field has myriad implications for its surface habitability (e.g., Driscoll and Bercovici, 2013; Foley and Driscoll, 2016) and the ongoing debate over the general relationship between magnetic shielding and atmospheric erosion (e.g., Tarduno et al., 2014).

Generally speaking, there are two basic requirements for a magnetic dynamo. First, the Coriolis force must strongly affect the fluid flow as indicated by a small Rossby number at the equator: $\mathrm{Ro} = v/(2L\Omega)$, where v is fluid velocity, L is the length scale of the dynamo region, and Ω is the angular rotation speed. Venus has the longest rotational period of the major planets, but $\mathrm{Ro} \approx 10^{-5} \ll 1$ (versus $\sim 10^{-6}$ for Earth) should still support dynamo action (e.g., Stevenson, 2003). Second, the magnetic Reynolds number $\mathrm{Re}_m = vL/\lambda$—where λ is magnetic diffusivity (inversely proportional to electrical conductivity)—must exceed a critical value $\sim$10–100. In the absence of other fluid motions like tidal stirring, this criterion mandates vigorous convection in a low viscosity (i.e., liquid) core. Dynamos constantly require energetic input—any global magnetic field would dissipate within $\sim 10^4$ yr after convection ceases (Stevenson, 2003).

Canonical models assume Venus has an "Earth-like" core—at least partially liquid and chemically homogeneous—that is currently cooling too slowly for a dynamo. Thermal convection only occurs if the heat flow across the core/mantle boundary (CMB)

* Corresponding author.
E-mail address: jgorourk@asu.edu (J.G. O'Rourke).

https://doi.org/10.1016/j.epsl.2018.08.055
0012-821X/

exceeds that which conduction would transport up an adiabatic temperature gradient. Nimmo (2002) argued that a transition from plate tectonics to the stagnant lid regime of mantle convection at ~500 Ma decreased CMB heat flow to nearly zero. Dramatic, global changes in mantle dynamics are commonly invoked to produce "catastrophic resurfacing" and explain the random distribution of impact craters on the surface (e.g., Strom et al., 1994; McKinnon et al., 1997). Ongoing debate over whether catastrophic resurfacing actually occurred hinges on the fraction of craters that suffered post-impact volcanic modification. Only ~10% of craters were classified as obviously embayed during the first analysis of radar images from Magellan (e.g., Strom et al., 1994). Monte Carlo models of cratering and non-catastrophic resurfacing can reproduce this low percentage (Bjonnes et al., 2012), but cannot explain the clustering of obviously embayed craters (O'Rourke et al., 2014). However, radar-dark floors found in ~80% of craters may indicate volcanic modification that is not otherwise obvious in low-resolution Magellan imagery (Wichman, 1999; Herrick and Rumpf, 2011). O'Rourke et al. (2014) showed that non-catastrophic resurfacing by thin, localized flows—matching some stratigraphic histories (Guest and Stofan, 1999)—would produce a volcanically modified population with the same size and spatial distributions as the dark-floored craters.

Even models without catastrophic resurfacing rely on low CMB heat flow to explain the absence of a dynamo today. One-dimensional, parametrized models agree that stagnant lid convection suppresses mantle and core cooling if melt migration to the surface is relatively inefficient (e.g., Stevenson et al., 1983; Solomatov and Moresi, 1996; Driscoll and Bercovici, 2013, 2014; O'Rourke and Korenaga, 2015; Foley and Driscoll, 2016). However, Armann and Tackley (2012) predicted that magmatic heat pipe dominates in the stagnant lid regime, which leads to unrealistically high rates of crustal production and Earth-like core/mantle heat flow. An episodic lid mode, in contrast, suppresses core cooling during quiescent periods and better matches the present-day amplitude of the geoid and topography. Recent work demonstrates that atmosphere–surface coupling causes transitions between different mantle convective regimes that ultimately stabilize surface conditions (Noack et al., 2012; Gillmann and Tackley, 2014). Factors affecting dynamo action have not been fully investigated in these new simulations.

Compositional buoyancy produced by chemical processes is potentially key to dynamo action in terrestrial planets. For example, the plausible range for the energy sink associated with thermal conduction in Earth's core (~4–11 TW) overlaps with the estimated ~5–15 TW total heat flux across the CMB today (Lay et al., 2008). There is no problem explaining Earth's dynamo at present, however, because exclusion of light elements from the solidifying inner core provides compositional buoyancy. Core/mantle heat flow need not exceed the conductive flux along the adiabat once the inner core nucleates since compositionally dense (but relatively hot) material can sink and carry heat downwards. Precipitation of light elements from the core may provide compositional buoyancy before nucleation of an inner core. O'Rourke and Stevenson (2016) first proposed that magnesium could provide an early power source for Earth's dynamo. Later, Badro et al. (2016) presented supportive results from diamond-anvil cell experiments. Magnesium is delivered in the ~10% of core-forming iron alloy that chemically equilibrates with mantle silicate at extremely high-temperature conditions in the aftermath of giant impacts. The solubility of magnesium in metal decreases rapidly with temperature, so cooling rates under ~50 K Gyr^{-1} still provide sufficient mass flux to drive convection. Hirose et al. (2017) subsequently suggested that crystallization of silicon dioxide may also occur at similar rates even if metal/silicate equilibration occurs at more moderate temperatures near mid-mantle depths. Additional mineral physics experiments are required to clarify many details about these new mechanisms. Regardless, Venus could possibly sustain a dynamo with sub-adiabatic heat flow in an Earth-like core even prior to inner core nucleation.

Two recent studies offer alternatives to canonical models of the core. First, Earth-sized planets are expected to form with stratified cores where the abundances of light elements increase with radius (Jacobson et al., 2017). Metal added later to the core during accretion chemically equilibrates with silicates at higher temperature/pressure conditions where silicon and oxygen are more soluble in metal. Earth's Moon-forming impact presumably eliminated this stratification through mechanical mixing. In the absence of a late energetic impact with appropriate geometry, this stratification may survive and completely prevent convection even with extremely rapid cooling. Second, the core of Venus may have completely solidified (e.g., Stevenson et al., 1983; Dumoulin et al., 2017). Doppler tracking of Magellan and Pioneer Venus Orbiter measured the tidal Love number as $k_2 = 0.295 \pm 0.066$ (Konopliv and Yoder, 1996). Elastic deformation models based on a one-dimensional seismological model of Earth's interior implied that a solid core would have $k_2 \approx 0.17$ compared to $0.23 < k_2 < 0.29$ for a liquid core (Konopliv and Yoder, 1996). However, Dumoulin et al. (2017) used a viscoelastic solution for mantle deformation to argue that the core must be fully solid if future spacecraft find $k_2 < 0.27$. Verifying either of these scenarios would profoundly alter theories for the accretion of Venus and Earth.

In this paper, we address two fundamental questions. First, does slow cooling alone explain the modern absence of a global magnetic field? Second, should we prioritize a search for crustal remanent magnetism on Venus? We run numerical simulations built on recent models of Earth's dynamo (O'Rourke and Stevenson, 2016; O'Rourke et al., 2017) and a previous investigation of coupled atmospheric and mantle dynamics on Venus (Gillmann and Tackley, 2014). For simplicity, we always assume that the core lacks significant compositional stratification and has an Earth-like bulk composition. Simulations that predict enough core cooling to drive a dynamo at present are taken as evidence for primordial stratification of the core (Jacobson et al., 2017), unless the core has completely solidified.

2. Model

Our simulations of the evolution of Venus include three modules to handle the energy balance of the atmosphere and the dynamics of the mantle and core. We consider two-way coupling between the atmosphere and mantle based on how melt production in the mantle releases greenhouse gases and then surface temperature determines the regime of mantle convection. This study includes some coupling between the mantle and core because the temperature of the core influences mantle convection, which controls the cooling rate of the core. However, we have not yet formulated a model for the influence of a magnetic field on atmospheric composition. Table 1 defines critical parameters that we use or track in our simulations, along with values for some important constants.

2.1. Evolution of the mantle

We continue to use the StagYY code to simulate mantle convection (Armann and Tackley, 2012; Gillmann and Tackley, 2014; Gillmann et al., 2016). Briefly, we assume a compressible, anelastic mantle with infinite Prandtl number in 2D, spherical annulus geometry with a resolution of 512 azimuthal by 64 radial cells plus 1 million tracers to track composition and melt fraction. Heat-producing elements are uniformly distributed initially but partition into melt as in some cases from Armann and Tackley (2012). We

Table 1
Definitions and default values for key parameters and constants used in our simulations. Terms describing the radial structure of the core were modified from Labrosse (2015).

Constant	Definition	Value	Units
C_p	Specific heat of the core	750	$kJ\,kg^{-1}\,K^{-1}$
$\partial T_L/\partial P$	Pressure dependence of the core liquidus	9	$K\,Pa^{-1}$
L_p	Length scale for the density profile in the core	8510	km
A_p	Prefactor in the density profile in the core	0.4835	
K_0	Bulk modulus in the density profile and liquidus	1172	GPa
r_c	Radius of the core	3110	km
Λ_m	Latent heat of MgO and/or SiO_2 crystallization	4	$MJ\,kg^{-1}$
α_m	Compositional expansitivity of MgO and/or SiO_2	0.8	
$\Delta\rho_p$	Density anomaly for the primordial layer	300	$kg\,m^{-3}$
σ_y	Yield stress at the surface	90	M Pa
$\partial\sigma_y/\partial z$	Increase in yield strength with depth	38.21	$Pa\,m^{-1}$

Parameter	Definition	Units
$\Delta\rho_0$	Density of pyroxene–garnet system relative to olivine	%
D_p	Thickness of the primordial layer in the lower mantle	km
C_m	Rate of MgO and/or SiO_2 precipitation	K^{-1}
k	Thermal conductivity at the center of the core	$W\,m^{-1}\,K^{-1}$
k_c	Minimum conductivity that prevents a modern dynamo	$W\,m^{-1}\,K^{-1}$
r_i	Radius of the inner core	km
ΔT_c	Initial "super-heat" in the core	K
T_{CMB}	Temperature at the core/mantle boundary	K
Q_{CMB}	Total core/mantle heat flow	TW
Q_S	Secular cooling of the core	TW
Q_R	Radiogenic heating in the core	TW
Q_L	Latent heat from inner core growth	TW
Q_G	Gravitational energy from inner core growth	TW
Q_C	Cooling of a perfectly conductive inner core	TW
Q_P	Gravitational energy from MgO and/or SiO_2 precipitation	TW
Q_E	Latent heat from MgO and/or SiO_2 precipitation	TW
Φ	Total dissipation in the core	TW
Φ_o	Dissipation produced at the core/mantle boundary	TW
Φ_i	Dissipation produced at the inner core boundary	TW
TDM	True dipole moment measured at the surface	$A\,m^2$

consider a single heat-producing component with an effective half-life of 2.43 Gyr and a globally averaged, radiogenic production rate of 5.2×10^{-12} $W\,kg^{-1}$ today (Armann and Tackley, 2012). Boundary conditions at the surface and CMB, respectively, are free slip and isothermal. The atmospheric model sets the surface temperature, whereas the core temperature evolves as a function of the core/mantle heat flux as described below. The initial temperature profile has small, random perturbations from an adiabat with a potential temperature of 1900 K and thin boundary layers at the top and bottom (Gillmann and Tackley, 2014).

Mantle material is initially a uniform mixture of two end-member components: basalt (20 wt%) and harzburgite (80 wt%). We assume that basalt consists of a pure pyroxene–garnet system, whereas harzburgite is composed of 25 wt% pyroxene–garnet and 75 wt% olivine (Armann and Tackley, 2012). Depth-dependent properties like density and thermal expansivity and conductivity—including phase transitions in both systems—are calculated as in Xie and Tackley (2004) and Armann and Tackley (2012). We vary the bulk modulus of the pyroxene–garnet system in the lower mantle, which creates a density difference that rises from zero at ~800 km depth to a maximum ($\Delta\rho_0 \approx$ 0–6%) near the CMB (e.g., Nakagawa and Tackley, 2014), to reflect the uncertainty in the density of basalt relative to harzburgite in the lower mantle (e.g., Hirose et al., 2005; Ohta et al., 2008). At each time step in the StagYY code, melt consisting entirely of basalt is removed from each cell if needed to return the temperature to the solidus. All melt generated above 300 km rises to the surface, but we assume that only 10% of the total melt production ends in extrusive volcanism. We also include a primordial layer of dense material above the CMB—presumably resulting from initial mantle differentiation (Nakagawa and Tackley, 2014)—with density equal to $\Delta\rho_p$ plus that of basalt at the CMB to reduce core/mantle heat flow at early times.

Rheology is assumed to be independent of composition and includes Newtonian diffusion creep plus plastic yielding (Gillmann and Tackley, 2014; Gillmann et al., 2016). The yield stress is the minimum of a brittle value predicted by Byerlee's law, with zero cohesion and a friction coefficient of 0.5, and a ductile yield stress, which is equal to 90 MPa at the surface but increases with depth to avoid unrealistic yielding in the lower mantle (Nakagawa and Tackley, 2015). In places where the stress is higher than the yield stress, the effective viscosity is iteratively adjusted to reduce it to the yield stress. In Armann and Tackley (2012), plastic yielding was favored to produce an episodic lid regime with realistic crustal thicknesses and volcanic activity instead of a stagnant lid regime with massive magmatism. No significant changes to the overall evolution were observed when ductile yield stress was varied between 80 and 120 MPa in coupled models (Gillmann and Tackley, 2014).

2.2. Evolution of the atmosphere

Our treatment of the atmosphere is nearly identical to the setup in Gillmann and Tackley (2014), which used a one-dimensional (vertical) model adapted from Phillips et al. (2001). Radiative transfer is grey, meaning that thermal infrared opacity depends on the altitude and abundance of greenhouse gases but not on wavelength. Self-consistent temperature profiles are calculated for a radiative layer and an underlying conductive layer that match at the tropopause, assuming hydrostatic equilibrium. Greenhouse gases CO_2 and H_2O are assumed to have constant mixing ratios with altitude. Solar flux increases over time from 70% of its present-day value at 4.5 Ga according to the faint young Sun hypothesis. Cloud evolution is not modeled in detail since we have not included a full, 3-D climate model. Effective temperatures are simply computed from the solar flux according to the black body law, as-

suming constant albedo (Gillmann and Tackley, 2014; Gillmann et al., 2016). Removing clouds at any time would decrease the planetary albedo and raise the surface temperature by several hundred degrees.

Greenhouse gases are removed by various escape processes, but replenished through mantle melting. To set the initial condition, we assume that hydrodynamic escape driven by extreme UV flux from the Sun caused fast H and O loss in the first ∼100 Myr after accretion. Rapidly drying the atmosphere decreases the surface temperature, which in turn speeds crystallization of the primordial magma ocean and can explain the present-day $^{20}Ne/^{22}Ne$ and $^{36}Ar/^{38}Ar$ ratios (Gillmann et al., 2009). A dense, CO_2 atmosphere with a partial pressure within ∼0.5–1% of the present-day value outgasses as the magma ocean solidifies. Subsequent melt production in our simulations barely increases atmospheric CO_2, although some degassing of H and CO may also occur in reality at early times. We assume that all volatiles in extrusive magma are degassed. However, we then use low apparent abundances of volatiles—e.g., a reduced mantle with only 125 ppm of CO_2 today—to compensate for the likelihood that high surface pressure prevents complete devolatilization on Venus (Elkins-Tanton et al., 2007; Gaillard and Scaillet, 2014). Escape of CO_2 is likewise negligible—currently below the detection limits of modern instruments (Gillmann and Tackley, 2014). Hydrodynamic escape always remains significant for H, but stops for O after ∼500 Myr as solar EUV flux drops. Various nonthermal escape processes involving solar emission and wind, which dominate atmospheric escape during the last ∼4 Gyr, are modeled at all times based on an energy-limited approach that takes into account evolution of solar EUV flux and present-day measurements (Gillmann and Tackley, 2014; Gillmann et al., 2016).

2.3. Evolution of the core

We make small modifications to a one-dimensional parameterization built for Earth on a fourth-order expansion of the radial density and gravity in the core (e.g., Labrosse, 2015; O'Rourke et al., 2017). Internal pressures are reduced relative to Earth by ∼7% and ∼20%, respectively, at the CMB and center of the core. Fig. 1 shows the implied liquidus temperatures in both planets. The core of Venus completely solidifies after ∼420 K of cooling once the inner core first nucleates (compared to ∼690 K for Earth). We assume that the outer core is chemically homogeneous and exhibits negligible deviations from an isentropic state except in thin boundary layers. In this case, the total heat flow across the CMB controls the thermal and chemical evolution of the core.

2.3.1. Calculating the total dissipation

Standard models for the evolution of metallic cores always include secular cooling (Q_S), radiogenic heating (Q_R), and two terms related to the growth of an inner core: latent heat of freezing (Q_L) and gravitational energy released from the exclusion of incompatible light elements (Q_G). Here we assume that Q_R results exclusively from the decay of potassium-40, although recent metal–silicate partitioning experiments also imply a small contribution from uranium (Chidester et al., 2017; Blanchard et al., 2017). If [K] = 200 ppm, then Q_R decays from 11.2 to 0.9 TW over 4.5 Gyr. Potassium is quite soluble in iron alloy, but experiments imply [K] < 100 ppm in Earth's core since potassium mostly partitions into silicates during equilibration at the base of a deep magma ocean (e.g., Hirose et al., 2013; Blanchard et al., 2017). We assume that the inner core has infinite thermal conductivity and maintains uniform temperature equal to the liquidus at its boundary. This introduces an additional cooling term:

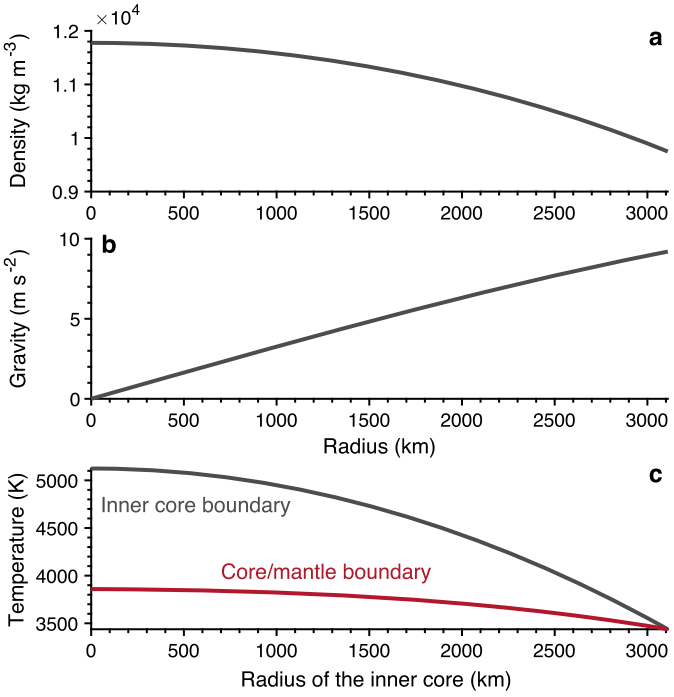

Fig. 1. Basic properties of our model for the core. Radial profiles of (a) density and (b) gravity. (c) Temperatures at the inner core and core/mantle boundaries associated with a given inner core radius. In similar models for Earth, the inner core nucleates and the core completely solidifies when the temperature at the core/mantle boundary drops below ∼4110 K and 3430 K, respectively (Labrosse, 2015).

$$Q_C = C_p M_{ic} K_0 \left(\frac{\partial T_L}{\partial P}\right)\left(\frac{2r_i}{L_p^2} + \frac{16r_i^3}{5L_p^5}\right)\left(\frac{dr_i}{dt}\right), \quad (1)$$

where M_{ic} is the mass of the inner core and K_0 is an effective bulk modulus (Labrosse, 2015). Other parameters are defined in Table 1. We could alternatively implement an insulating inner core with an adiabatic temperature gradient by setting $Q_C = 0$ TW.

Precipitation of buoyant components like MgO and/or SiO_2 may begin at a critical temperature and continue thenceforth with a nearly steady mass flux (e.g., O'Rourke and Stevenson, 2016; Badro et al., 2016; Hirose et al., 2017). In this study, we model a fiducial light component because of uncertainties about the exact partitioning behavior and relative abundances of each element (e.g., Du et al., 2017). This formulation covers many plausible scenarios that are energetically equivalent. We calculate the resulting contribution to the total heat budget from gravitational energy as

$$Q_P = \frac{8}{3}\pi^2 G \rho_0^2 L_p^5 \alpha_m C_m \left[f_\gamma\left(\frac{r_c}{L_p}\right) - f_\gamma\left(\frac{r_i}{L_p}\right)\right]\frac{dT_{CMB}}{dt}, \quad (2)$$

where the useful function

$$f_\gamma(x) = x^3\left[-\frac{\Gamma}{3} + \frac{(1+\Gamma)x^2}{5} + \frac{(A_p\Gamma - 1.3)x^4}{6}\right], \quad (3)$$

with $\Gamma = (r_c/L_p)^2[1 - 0.3(r_c/L_p)^2]$. We also include a latent heat $Q_E = \Lambda_m C_m M_{oc}(dT_{CMB}/dt)$, where M_{oc} is the mass of the outer core, associated with crystallization of the light components at the CMB. Remarkably, independent experiments indicate that $C_m \approx 2 \times 10^{-5}$ K^{-1} for both MgO and SiO_2 precipitation, so our simulations are not sensitive to the exact composition of the precipitate. Energetic impacts during accretion are necessary to deliver ∼1–3 wt% MgO into the core (Badro et al., 2016). If giant impacts are also required to disrupt primordial stratification (Jacobson et al., 2017), then any Earth-sized core that is able to convect should experience MgO precipitation. However, SiO_2 exsolution is possible

even if metal/silicate equilibration during core formation primarily occurred near liquidus temperatures at mid-mantle depths and the initial abundance of Mg is negligible (Hirose et al., 2017).

The global energy budget is simply the sum of all the heat sources (e.g., Labrosse, 2015). That is,

$$Q_{CMB} = Q_S + Q_R + Q_P + Q_E + Q_L + Q_C + Q_G. \quad (4)$$

We assume that the core begins with a "hot start," where initial temperature is elevated relative to the basal mantle (e.g., Stevenson et al., 1983). Specifically, the initial temperature equals 4121 K—slightly above the temperature at which inner core growth begins (3859 K)—plus an additional ΔT_c. The cooling rate of the core is hence

$$\frac{dT_{CMB}}{dt} = \frac{Q_{CMB} - Q_R}{\widetilde{Q}_S + \widetilde{Q}_P + \widetilde{Q}_E + \widetilde{Q}_L + \widetilde{Q}_C + \widetilde{Q}_G}, \quad (5)$$

where $\widetilde{Q}_i = Q_i/(dT_{CMB}/dt)$ are calculated analytically (Labrosse, 2015). The total dissipation includes all these terms multiplied by appropriate efficiency factors, plus a sink term related to heat conduction along the adiabatic gradient. We can write the total dissipation as $\Phi = \Phi_i + \Phi_o$, where we calculate contributions from the inner and outer boundaries, respectively, as in Aubert et al. (2009):

$$\Phi_i = \frac{T_D(T_L - T_{CMB})}{T_L T_{CMB}}(Q_L + Q_C) + \frac{T_D}{T_{CMB}} Q_G \quad (6)$$

and

$$\Phi_o = \frac{T_D(T_R - T_{CMB})}{T_R T_{CMB}} Q_R + \frac{T_D(T_S - T_{CMB})}{T_S T_{CMB}} Q_S + \frac{T_D}{T_{CMB}} Q_P - T_D E_K. \quad (7)$$

The effective temperature of dissipation overall is T_D, which is calculated along with other terms not defined here exactly as in Labrosse (2015). All heat sources except those related to compositional buoyancy (Q_G and Q_P) are hampered by a "Carnot-like" efficiency term. Those sources with lower effective temperatures (e.g., $T_R < T_S < T_L$) produce relatively less dissipation. We omitted any term related to Q_E since heat sources at the CMB contribute nothing to the dissipation (i.e., $T_E - T_{CMB} = 0$ K). The minimum requirement for a dynamo is $\Phi > 0$ TW. The actual Ohmic dissipation produced by Earth's dynamo is uncertain, but possibly as high as ~3–8 TW (Stelzer and Jackson, 2013). We predict the true dipole moment (TDM) over time using a scaling law for a strong-field, dipole-dominated dynamo from Aubert et al. (2009) as detailed in the supplementary material.

The thermal conductivity of iron alloys under extreme temperature and pressure conditions is currently uncertain by a factor of two to three. Extrapolations of theory and experiments applicable to lower pressure and temperature conditions predicted values around $\lesssim$40–50 W m^{-1} K^{-1} in Earth's core (e.g., Stacey and Loper, 2007). However, recent first-principles calculations (de Koker et al., 2012; Pozzo et al., 2012) and diamond-anvil cell experiments (Gomi et al., 2013; Seagle et al., 2013; Ohta et al., 2016) suggest that the electrical resistivity at core conditions is several times lower than previously believed. Thermal conductivity was thus calculated as $\gtrsim$90–130 W m^{-1} K^{-1} at the CMB, increasing to ~150–200 W m^{-1} K^{-1} at Earth's inner core boundary according to the Wiedemann–Franz "law". However, direct measurements of thermal conductivity in diamond-anvil cells suggest that this empirical relation may not hold at core conditions, and the earlier estimates of conductivity (~40–50 W m^{-1} K^{-1}) are possibly still valid (Konôpková et al., 2016). Because thermal conductivity does not appear in the global heat budget, we can quickly re-compute the predicted dissipation for the entire range of plausible values—always assuming the depth dependence from Labrosse (2015) where the average conductivity equals ~0.7k—without repeating a full simulation. In particular, we calculate the minimum thermal conductivity (k_c) at the center that prevents positive dissipation at present day for each simulation.

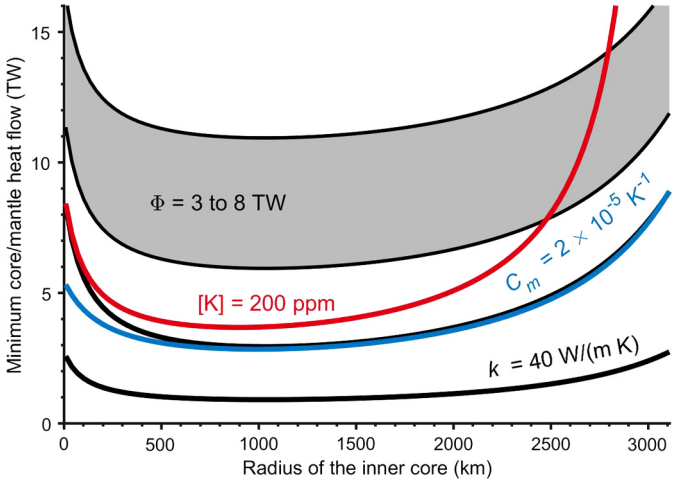

Fig. 2. Minimum total core/mantle heat flow required to drive a dynamo for various values of thermal conductivity at the center of the core and total Ohmic dissipation, assuming Venus has an "Earth-like" core that is chemically homogeneous and fully convective except in thin boundary layers. Except where otherwise labeled, we assume $\Phi = 0$ TW, $C_m = 0$ K^{-1}, [K] = 0 ppm, and $k = 130$ W m^{-1} K^{-1} as for the unlabeled, black curve. They gray, shaded region denotes heat flows required to maintain $\Phi = 3$–8 TW. The red curve shows a calculation with [K] = 200 ppm, while the blue curve has $C_m = 2 \times 10^{-5}$ K^{-1}. The lowest, black curve has k reduced to 40 W m^{-1} K^{-1}. (For interpretation of the colors in the figure(s), the reader is referred to the web version of this article.)

Fig. 2 shows the minimum Q_{CMB} required to produce a dynamo under various conditions. If the low values of thermal conductivity are correct, then the minimum Q_{CMB} drops from ~2.5 to only 1 TW once the inner core nucleates. Increasing the thermal conductivity to the upper estimates increases the power requirements by ~3.4 times. Likewise, raising Φ to reflect non-zero Ohmic dissipation causes an identical increase in the required heat flow. The minimum Q_{CMB} is incrementally boosted for small r_i but skyrockets for $r_i > 2500$ km with any radiogenic elements under our assumption that they are incompatible in the inner core. Adding MgO and/or SiO_2 precipitation roughly halves the required Q_{CMB} prior to inner core nucleation but negligibly reduces it once $r_i \gtrsim 750$ km. Similarly, inner core nucleation only decreases the minimum Q_{CMB} by ~50% if precipitation is already ongoing.

3. Results

Table 2 lists input parameters and key output results from forty simulations. Numbers 1 through 34 use the full atmosphere–mantle coupling described above (Gillmann and Tackley, 2014). We first consider the possibility that Venus currently hosts a liquid outer core like Earth, which simply loses heat by conduction without rapid fluid motions. Then, we determine the initial conditions that permit the core to have completely solidified with simulations 32–34. We mostly discuss simulations 35–40 in the supplementary material.

3.1. Insufficient cooling of an "Earth-like" core

3.1.1. Example simulation

Representative results are obtained with slight modifications to the preferred atmospheric and mantle evolution from Gillmann and Tackley (2014) in simulation 8 from Table 2. Atmospheric abundances of CO_2 and H_2O are initially 84.5 bar and 2.7 mbar, respectively. Basalt is set as 3% more dense than harzburgite at

Table 2
Initial conditions and key output results for every simulation performed for this study. Important values include the time of inner core nucleation (t_i), the total heat flow from the mantle through the surface (Q_M), and the thickness of crust produced since 750 Ma (Δh_c). ⋆Simulations 35–37 have atmosphere–interior coupling but $\sigma_y = 300$ MPa so that recent evolution is in the stagnant (instead of episodic) lid regime. †Simulations 38–40 have no atmosphere–interior coupling—the surface temperature is fixed to 740 K with $\sigma_y = 90$ MPa so that Venus always evolves in the episodic lid regime.

#	$\Delta\rho_0$ (%)	D_p (km)	ΔT_c (K)	[K] (ppm)	C_m (10^{-5} K^{-1})	t_i (Gyr)	Δh_c (km)	$Q_M(t_p)$ (TW)	$Q_{CMB}(t_p)$ (TW)	$r_i(t_p)$ (km)	k_c (W m^{-1} K^{-1})
1	0	0	1000	0	2	1.2	3.7	13.5	8.9	2877	176
2	0	200	1000	0	2	2.3	9.1	15.6	5.6	1851	220
3	0	400	1000	0	2	1.9	3.5	13.9	3.1	1922	120
4	6	0	1000	0	2	1.4	8.5	17.9	3.3	2198	110
5	6	200	1000	0	2	1.6	4.9	15.8	3.0	1974	111
6	6	400	1000	0	2	1.5	8.4	15.1	1.2	2052	44
7	3	0	1000	0	2	1.4	7.3	17.5	4.3	2306	135
8	3	200	1000	0	2	2.0	4.8	15.4	2.7	1654	113
9	3	400	1000	0	2	1.8	6.7	20.1	3.8	1847	150
10	6	200	1000	200	2	1.9	8.9	20.3	5.0	1661	164
11	6	200	1000	400	2	2.6	9.9	17.3	3.9	1233	102
12	6	200	1000	600	2	3.7	12.4	25.1	7.6	889	252
13	0	200	2000	0	2	2.7	12.5	24.8	7.3	1670	304
14	3	200	2000	0	2	2.4	6.7	15.5	4.1	1666	171
15	6	200	2000	0	2	1.8	12.5	15.2	5.4	1946	205
16	0	200	2000	200	2	3.4	10.3	15.8	6.2	1383	236
17	3	200	2000	200	2	3.2	5.9	18.0	5.1	1298	191
18	6	200	2000	200	2	2.2	10.8	17.2	4.8	1701	155
19	0	400	2000	200	2	3.4	9.3	16.5	6.2	1329	240
20	3	400	2000	200	2	2.7	7.9	17.0	5.9	1551	213
21	0	200	1000	200	2	3.4	14.3	16.8	5.7	1340	218
22	0	200	1000	400	2	4.3	5.5	13.5	7.6	619	276
23	0	200	1000	600	2	>4.5	44.3	14.7	7.6	0	154
24	3	200	1000	50	2	2.2	7.7	17.6	4.0	1596	159
25	3	200	1000	100	2	2.4	7.7	17.2	4.5	1480	177
26	3	200	1000	200	2	2.9	5.7	16.6	3.5	1248	122
27	3	200	1000	400	2	4.0	7.6	16.7	5.8	814	202
28	3	200	1000	600	2	>4.5	7.5	19.7	5.5	0	105
29	6	0	1000	0	0	1.3	8.1	16.4	3.4	2295	104
30	6	200	1000	0	0	1.4	7.5	15.4	1.7	2070	59
31	6	400	1000	0	0	1.4	7.2	16.1	1.3	2214	42
32	6	200	0	0	0	0.9	8.9	22.8	1.0	2348	30
33	6	0	0	0	0	0.5	10.0	19.7	1.6	2412	47
34	0	0	0	0	0	0.5	13.0	14.6	6.0	3110	–
35⋆	0	200	1000	0	2	1.9	32.3	10.4	4.9	2014	179
36⋆	3	200	1000	0	2	1.9	12.5	12.0	1.7	1635	73
37⋆	6	200	1000	0	2	1.4	12.8	11.4	1.9	2186	65
38†	0	200	1000	0	2	2.7	6.2	14.9	5.8	1755	232
39†	3	200	1000	0	2	2.6	6.8	21.1	6.9	1640	289
40†	6	200	1000	0	2	1.6	9.4	35.5	3.6	2040	129

the CMB. We include a primordial, dense layer with a thickness of 200 km to insulate the core at early times. The initial temperature of the core is 5092 K and [K] = 0 ppm. Precipitation of MgO and/or SiO_2 occurs at constant $C_m = 2 \times 10^{-5}$ K at temperatures below 4500 K. Fig. 3 contains snapshots of the mantle temperature and composition at 1 Gyr intervals, while Fig. 4 illustrates the radial temperature profiles in the mantle at these time steps. Fig. 5 shows the detailed evolution of many critical parameters.

Partial melting produces a surface layer of basaltic crust within ∼20 Myr after the simulation starts. Around ∼200 Myr, an era of rapid magmatism begins as plumes upwell from the CMB while slab-like downwelling events occur periodically across the entire mantle (Gillmann and Tackley, 2014). Primordial material mostly remains at the CMB, although a small amount is entrained and transported upwards—but not above the 730 km phase transition (equivalent to 660 km in Earth). Horizontal velocities near the surface are typically 0.01–0.1 cm yr^{-1}, but can reach an order of magnitude larger during resurfacing events. Sluggish horizontal velocities and increasing mantle temperatures are characteristic of the stagnant lid regime (Gillmann and Tackley, 2014). Despite the rapid melt production and ongoing release of greenhouse gases, surface temperature decreases from ∼1070 to 730 K at ∼960 Myr as solar EUV flux reduces atmospheric [H_2O] to 0.01 mbar.

Low surface temperatures facilitate the transition at ∼960 Myr to a mobile lid regime resembling plate tectonics. Increased viscosity in the (colder) upper mantle makes convective stress relatively more likely to exceed the yield stress in viscoplastic rheology. During this second stage, typical horizontal velocities are a few cm yr^{-1} with few quiescent periods. Mantle melting causes transient jumps in [H_2O] correlated with spikes in surface temperature from a ∼520 K minimum. Mantle temperatures quickly decrease at first as surface heat flow rises, but remain roughly constant during the second half of this stage. Starting around ∼1.7 Gyr, water vapor begins to accumulate in the atmosphere as escape processes become less efficient (Gillmann and Tackley, 2014). Mantle dynamics then enter a third stage where surface temperatures rise and the mobile lid gradually stagnates. Melt production drops as convective velocities decrease. After ∼2.3 Gyr, the fourth and final stage starts as surface temperature levels off near the present-day 740 K. An episodic lid regime begins that features several prominent spikes in surface heat flow associated with localized resurfacing events—but not global, catastrophic resurfacing.

At the end of the simulation, a layer of basalt ∼1000 km thick has built up above the CMB—a typical outcome of crustal overturns in the episodic lid regime. The basaltic layer is much thinner in simulations with continuous subduction or perpetual evolution in the stagnant lid regime (Nakagawa and Tackley, 2015). The core/mantle temperature contrast calculated from an adiabat projected down from the 730 km phase transition in the mantle is similar to the ∼500–1000 K inferred for Earth today. However, ra-

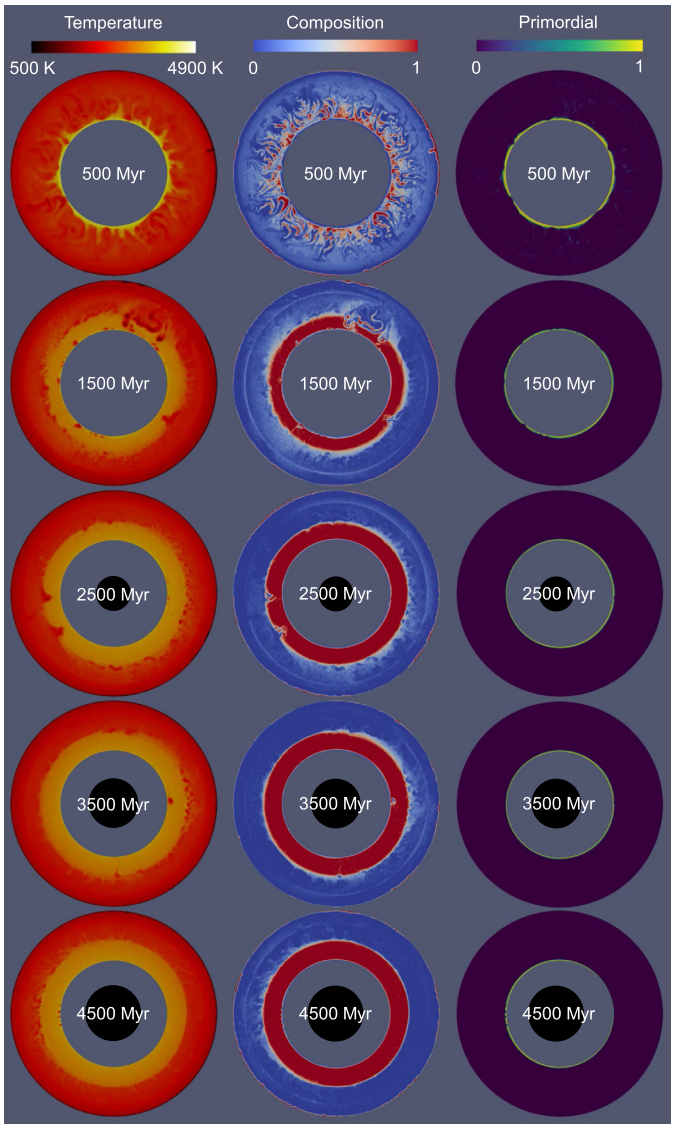

Fig. 3. Snapshots of temperature (left), composition (center), and concentration of primordial material (right) in the mantle for our example simulation. Composition ranges from 0 (harzburgite) to 1 (basalt), with the primordial material colored as harzburgite in the center column and in yellow on the right. The inner core is drawn to scale as a black circle at each time step.

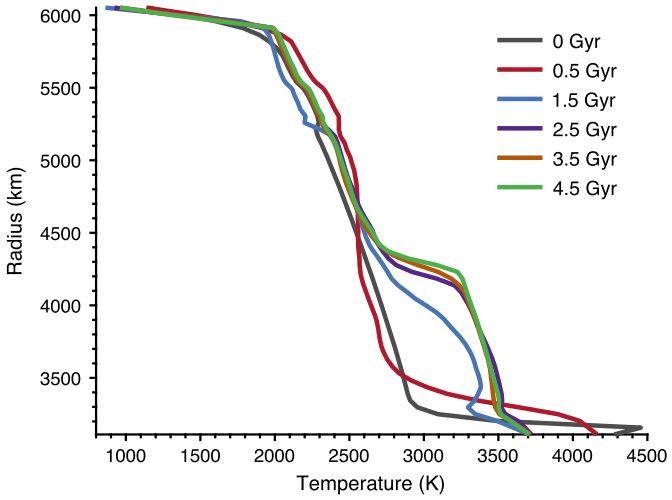

Fig. 4. Radial profiles of temperature in the mantle at the beginning of our example simulation and at the time steps depicted in Fig. 3.

diogenic heating in the basaltic layer raises the temperatures in the lower mantle by an additional ∼500 K. Therefore, as seen in Fig. 4, the temperature contrast through the lowest boundary layer in the mantle (i.e., the primordial layer) is only ∼200 K at the end of this simulation.

Each stage of atmosphere–mantle evolution profoundly affects the likelihood of dynamo action in an "Earth-like" core. Core cooling declines from ∼47 to 21 TW during the first stage as the CMB temperature contrast rapidly drops. Thermal convection alone sustains a magnetic dynamo with Earth-like surface strength even before MgO/SiO_2 precipitation increases Φ by ∼50% at ∼600 Myr. Fig. 6 shows that $Q_P \approx 0.1 Q_S$ at this time, but both terms contribute nearly identical amounts of dissipation since precipitation is not penalized by a "Carnot-like" efficiency. During the mobile lid stage, core/mantle heat flow rises to oscillate around ∼30–40 TW. The inner core nucleates shortly after this stage, which more than doubles Φ but barely affects the predicted TDM since the dynamo becomes deeper seated (Aubert et al., 2009; Landeau et al., 2017). Inner core growth contributes more to the heat budget than both precipitation and secular cooling—and thus becomes the dominant source of dissipation. The effective temperatures of dissipation (T_D, et al.) slowly decrease to remain between the temperatures at the core/mantle and inner core boundaries. Fig. 6 also shows that the sink term associated with thermal conduction (and, less obviously, all terms) gradually decreases in response.

Core/mantle heat flow begins a steady decline once the mantle reenters the stagnant lid regime, reaching only 2.7 TW at present day. Still, Earth-like field strengths are predicted at the surface continuously until ∼4 Gyr. Three regional resurfacing events between ∼2.3 and 3 Gyr deliver relatively cold material to the cold/mantle boundary. Associated small spikes in Q_{CMB} and thus Φ and TDM appear ∼100 Myr (the mantle transit time) after surface heat flow reaches a local maximum. Fig. 5 shows that a burst of dynamo activity is predicted to occur between ∼200–100 Ma if the thermal conductivity is $k_c = 113\ \mathrm{W\,m^{-1}\,K^{-1}}$. This burst is not suppressed even if k is raised to $130\ \mathrm{W\,m^{-1}\,K^{-1}}$—the upper end of modern estimates. In contrast, if the lowest estimates for thermal conductivity (∼40–50 $\mathrm{W\,m^{-1}\,K^{-1}}$) prove correct, then an "Earth-like" core is obviously incompatible with the modern lack of a dynamo. Increasing k from 40 to $130\ \mathrm{W\,m^{-1}\,K^{-1}}$ bolsters the dissipative sink by ∼1 TW. This absolute change only corresponds to a large proportional change when Φ is small since TDM $\propto \Phi^{0.34}$ in our scaling. Therefore, k strongly affects TDM in recent times but not before ∼2 Gyr.

3.1.2. Sensitivity tests

We now test plausible values for parameters that are likely to strongly affect the dynamo while still producing realistic atmospheric evolution and surface volcanism. Varying the basalt–harzburgite density contrast at the CMB is the only change that appreciably affects the compositional structure of the mantle in this study. Fig. 7 illustrates that any $\Delta\rho_0 \gtrsim 3\%$ will produce a thick, basal layer of basalt. When basalt and harzburgite have similar densities in the lower mantle, slab-like downwellings are more likely to reach the CMB. A thick layer of basalt should reduce core/mantle heat flow—present-day $Q_{CMB} = 8.9$, 4.3, and 3.3 TW for [K] = 0 ppm, $D_p = 0$ km, and $\Delta\rho_0 = 0$, 3, and 6%, respectively—although this general trend does not always hold because of the variable timing and magnitude of regional downwellings during the episodic lid phase.

Fig. 8 shows how the critical conductivity that suppresses recent dynamo activity depends on various parameters for simulations 1 through 33. One correlation is immediately obvious: simulations that predict Earth-like $Q_{CMB} > 5$ TW are incompatible with Venus having an "Earth-like" core but no dynamo today, as-

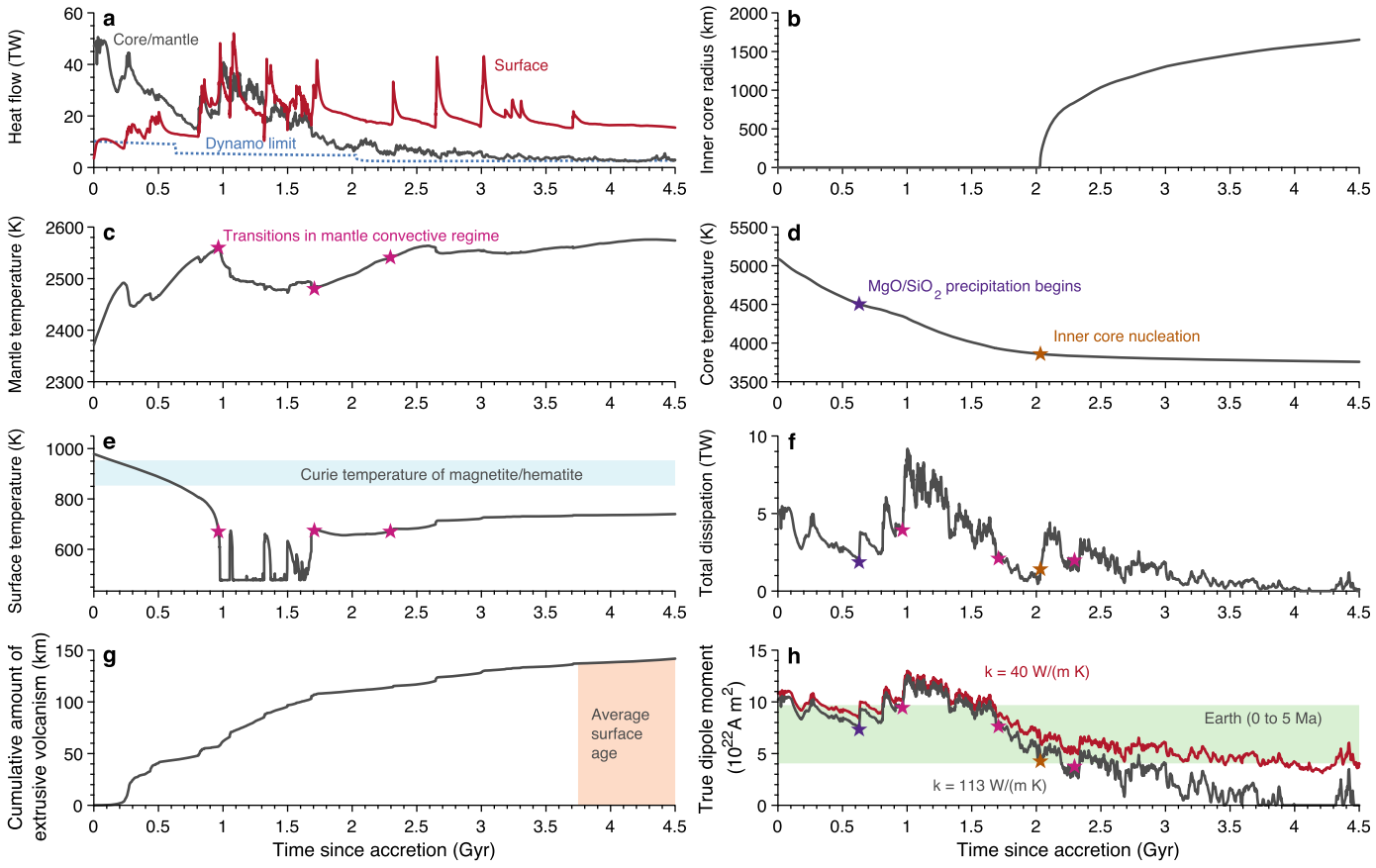

Fig. 5. Evolution of Venus in our example simulation. (a) Surface heat flow (red) compared to the actual heat flow across the CMB (black) and the minimum necessary to drive a dynamo (blue, dotted) if $k = k_c = 113\ \mathrm{W\,m^{-1}\,K^{-1}}$ at the center. (b) Radius of the inner core. (c) Volume-averaged temperature in the mantle. Pink stars denote transitions in the regime of mantle convection from stagnant lid to mobile lid, then gradually to stagnant lid again, followed by episodic lid until the present. (d) Temperature at the core/mantle boundary. The purple and orange stars indicate the temperatures corresponding to the onset of MgO and/or SiO_2 precipitation and the nucleation of the inner core, respectively. (e) Surface temperature proportionally rescaled (i.e., multiplied by 0.9172) to equal exactly 740 K today. The blue, shaded region shows the range of Curie temperatures for magnetite and hematite. (f) Total dissipation produced in the core, assuming $k = k_c$. (g) Extrusive portion (10%) of the total melt production, converted into an equivalent depth of surface volcanism. The orange shaded area indicates the ~750 Ma estimate for the average surface age (McKinnon et al., 1997). The amount of volcanism produced during this time period corresponds to an effective depth of ~1.5 km. (h) Predicted TDM over time for $k = k_c$ (grey) and $k = 40\ \mathrm{W\,m^{-1}\,K^{-1}}$ (red). The green, shaded region is the "1-sigma" range of paleointensities for Earth in the 0.05–5 Ma time interval (Smirnov et al., 2016). The predicted TDM is always either zero or larger than the non-detection limit from orbiting magnetometers (Phillips and Russell, 1987).

suming $k \leq 160\ \mathrm{W\,m^{-1}\,K^{-1}}$ in reality. This excludes $\Delta T_c > 1000$ K and, in most cases, [K] $\geq$ 100 ppm. One simulation with [K] = 600 ppm has $k_c < 110\ \mathrm{W\,m^{-1}\,K^{-1}}$ because nucleation of the inner core never occurs. Otherwise, some inner core growth seems inevitable because the core cools rapidly during the first three stages of mantle dynamics. More rapid cooling in the past implies slower cooling today, so inner core radius is anticorrelated with Q_{CMB} at present day. Eliminating MgO and/or SiO_2 precipitation (perhaps by forming a reduced core with Si but little O) hastens nucleation of the inner core by increasing $\mathrm{d}T_{CMB}/\mathrm{d}t$ for a given Q_{CMB}. Therefore, depriving Venus of these power sources would not by itself substantially raise k_c and thus explain the absence of a modern dynamo.

The supplementary material includes detailed descriptions of simulations 35–40 alongside simple, parameterized models of thermal evolution (e.g., O'Rourke and Korenaga, 2015). First, we increased the yield stress to 300 MPa in simulations 35–37 to force the mantle into the stagnant lid regime after a transition away from the mobile lid regime near ~1.5 Gyr. We found that CMB heat flow was suppressed at present day—which lowered k_c by $\sim 40\ \mathrm{W\,m^{-1}\,K^{-1}}$ and decreased the likelihood of a present-day dynamo—relative to simulations where the mantle is now in a quiescent period between episodic resurfacing events. Second, we ran simulations 38–40 with a constant surface temperature equal to the present-day 740 K to examine perpetual evolution in the episodic lid regime. Without a period of rapid heat loss in the mobile lid regime, we found that the mantle tends to cool down rather than heat up in recent times. This promotes increased core cooling and would render an "Earth-like" core incompatible with the lack of a modern dynamo unless $k \gtrsim 130\ \mathrm{W\,m^{-1}\,K^{-1}}$.

3.2. Complete solidification of an "Earth-like" core

Complete solidification of the core in our simulations requires eliminating the primordial layer and any basalt/harzburgite density anomaly, along with lowering the initial temperature and removing other heat sources from our simulations. For instance, we repeated simulation 5 ($\Delta\rho_0 = 6\%$ and $D_p = 200$ km) with ΔT_c lowered to 0 K as simulation 32, but the inner core only grew to 2348 km at present day. Removing the primordial layer only increased the final r_i by 64 km (simulation 33). In simulation 34, the core finally solidified after ~4.4 Gyr once we also set $\Delta\rho_0 = 0\%$. Implementing a completely insulating inner core with $Q_C = 0$ TW might allow complete solidification for small values of D_p or $\Delta\rho_0$, but we expect a minor effect since $Q_C \lesssim 0.25(Q_L + Q_G)$ in general. Complete solidification will not occur in any simulation with [K] > 0 ppm unless we change the assumed partitioning behavior to segregate potassium in the inner core or mantle at lower temperatures. We omit simulations with $\Delta T_c < 0$ K because any scenario for accre-

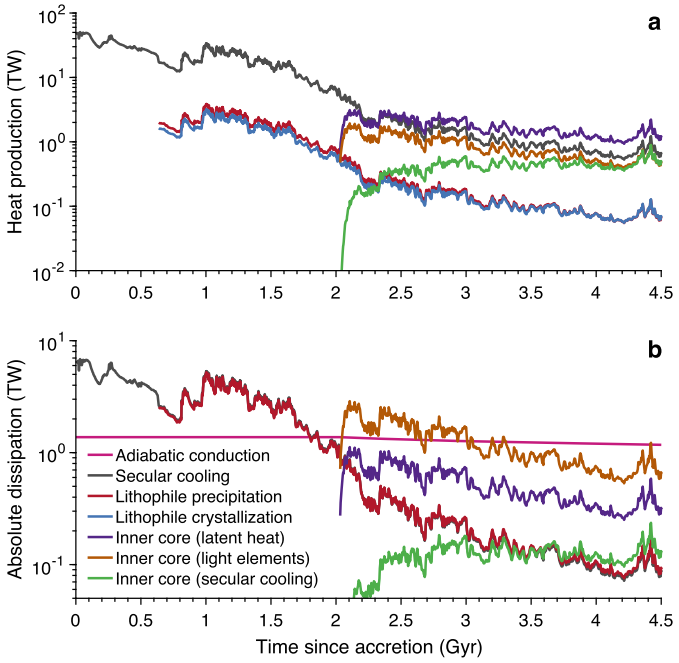

Fig. 6. Details about heat production and dissipation in the core from our example simulation. (a) Heat production associated with secular cooling (Q_S), precipitation of MgO and/or SiO_2 (Q_P), crystallization of the light component (Q_E), and inner core growth (Q_L, Q_G, and Q_C for latent heat, gravitational energy, and secular cooling, respectively). (b) Total dissipation associated with these six sources compared to the term related to conductive heat flow along the adiabatic gradient computed assuming $k = k_c = 113\ \mathrm{W\,m^{-1}\,K^{-1}}$.

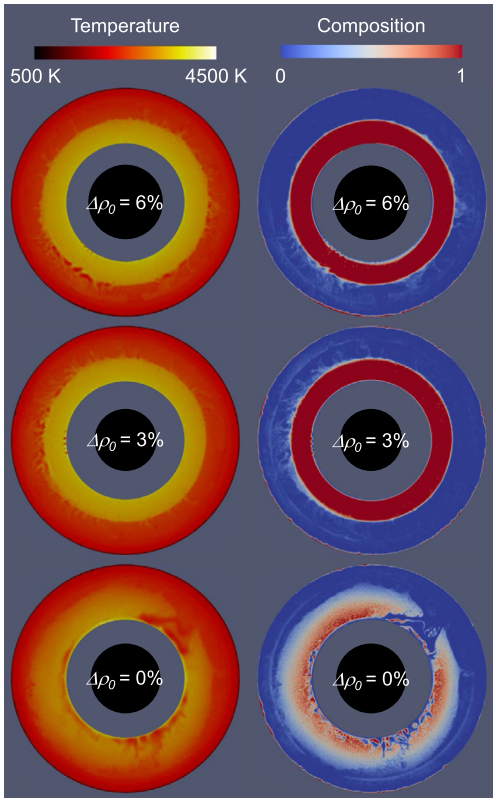

Fig. 7. Effects of a basalt/harzburgite density contrast in the lower mantle. Temperatures (left) and composition (right) are shown at the end of three simulations with $\Delta\rho_0 = 6$, 3, and 0% (top to bottom). A basal, primordial layer is included in each simulation and colored as harzburgite in the right column. Inner cores are again drawn to scale as black circles.

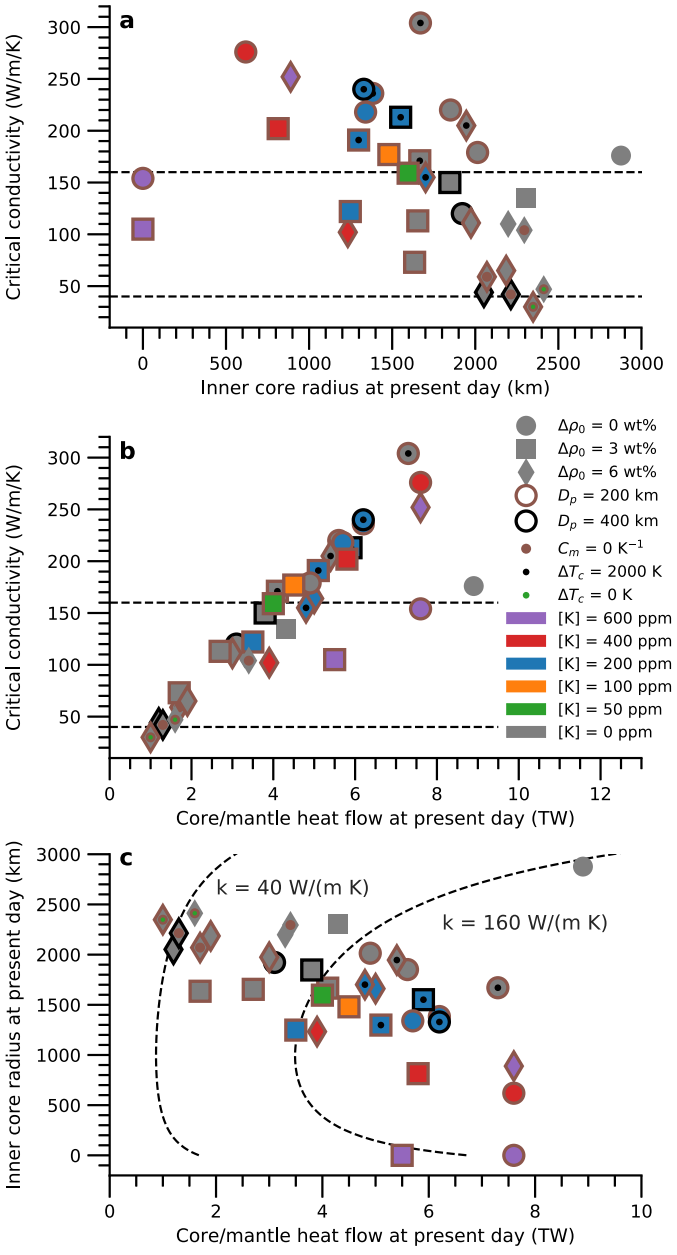

Fig. 8. Correlations between the critical conductivity for recent dynamo action and the present-day values of the inner core radius and core/mantle heat flow. Symbol shapes represent different assumed values of $\Delta\rho_0$, while colors show the prescribed [K]. Solid, brown and black borders indicate simulations with $D_p = 200$ km and 400 km instead 0 km, respectively. Black or green circles plotted inside a symbol indicate that $\Delta T_c = 2000$ K or 0 K, respectively, instead of the usual 1000 K. Slightly larger, brown circles plotted inside the main symbol indicate $C_m = 0\ \mathrm{K^{-1}}$ instead of $2 \times 10^{-5}\ \mathrm{K^{-1}}$). Dashed curves (c) show the minimum CMB heat flow necessary to drive a modern dynamo assuming $\Phi = 0$ TW, $C_m = 2 \times 10^{-5}\ \mathrm{K^{-1}}$, and [K] = 0 ppm for the upper and lower bounds on thermal conductivity.

tion that initially produces very cold conditions is likely to create substantial compositional stratification.

4. Conclusions

We presented numerical simulations of the coupled evolution of the atmosphere, surface, mantle, and core of Venus. Our main conclusions are as follows:

1. If the lowest estimates for thermal conductivity (~40–50 $\mathrm{W\,m^{-1}\,K^{-1}}$) are confirmed, then the core of Venus must have

completely solidified (Dumoulin et al., 2017) or preserved primordial compositional stratification (Jacobson et al., 2017). Complete solidification of an initially liquid core necessitates the absence of radiogenic heating and any dense, basaltic layer that would insulate the core/mantle boundary. Low initial temperatures are also required, and a cold core might form with compositional stratification anyways. Higher conductivities (e.g., >100 W m^{-1} K^{-1}) are consistent with the conventional view that Venus has an "Earth-like" core that is cooling too slowly to convect if a thick layer of primordial, dense material ($D_p \geq 200$ km) and/or recycled basalt ($\Delta\rho_0 \geq 3\%$) insulates the CMB at present.

2. Future spacecraft missions could detect crustal remanent magnetism on Venus, which would support similar conditions during the accretion of Venus and Earth. The surface of Venus is likely covered in basaltic flows, which contain magnetite when fresh that weathers to hematite (e.g., Gilmore et al., 2017). Our atmospheric model predicts that the surface has remained below the Curie temperatures of these common magnetic minerals for at least ~2 Gyr. Successful simulations with an "Earth-like" core predict continuous dynamo activity for ~4 Gyr, and often intermittent magnetism over the last 500 Myr for conductivities above the critical value for a modern dynamo. Magnetized rocks should be found on or near the surface since crustal temperatures quickly increase to the Curie point with depth and hot lava flows are responsible for the vast majority of resurfacing.
3. Heat loss from the mantle of Venus during quiescent periods in the episodic lid regime is reduced to less than half the modern value for Earth, e.g., ~15 versus 44 TW, which matches observational constraints (e.g., O'Rourke and Smrekar, 2018). Therefore, the mantle of Venus is possibly heating up today (e.g., Smrekar and Sotin, 2012), but this does not completely suppress core cooling. Our simulations still predict >2 TW of core/mantle heat flow for Venus since a "hot start" for the core maintains a significant temperature contrast across the CMB over geologic time. Every 200 ppm of potassium added to the core increases the predicted CMB heat flow by ~2 TW at present day.
4. If the core actually contains >200 ppm of potassium, then our simulations indicate that a dynamo would probably exist today if there was no primordial, compositional stratification. Concentrations in the range ~400–800 ppm are commonly invoked in models of Earth's evolution to prevent the inner core from growing larger than its present-day size while cooling remains fast enough at early times to sustain a dynamo given high thermal conductivity (e.g., Nakagawa and Tackley, 2010, 2014; Driscoll and Bercovici, 2014). But mineral physics experiments seem to favor [K] < 50–100 ppm for Earth's core based on the affinity of potassium for silicates instead of iron alloy (e.g., Hirose et al., 2013; Blanchard et al., 2017). Little to no radiogenic heating is required for Earth's core if the heat flow is only ~5–10 TW at present and precipitation of MgO and/or SiO_2 drove compositional convection at early times (e.g., O'Rourke et al., 2017).
5. Future work should consider a plethora of additional processes, and some alternative scenarios for the evolution of Venus. Viscosity in the lower mantle, which has a somewhat uncertain sensitivity to temperature, regulates core cooling. Tessera terrain are possibly composed of large volumes of felsic melts, which may require ocean-sized quantities of liquid water to form (e.g., Gilmore et al., 2017). Here we assume that solar EUV flux dried out the atmosphere and surface quickly after accretion. But oceans are possibly stable for billions of years on Venus if they did form (Way et al., 2016), which may favor a prolonged mobile lid regime and more rapid core cooling. A global magnetic field may strongly affect atmospheric evolution with or without condensed oceans, so integrating two-way atmosphere/core coupling into numerical simulations remains a priority.

Acknowledgements

J.G. O'Rourke is supported by an ASU SESE Exploration Postdoctoral Fellowship. C. Gillmann was supported by BELSPO's Planet TOPERS IAP programme and FNRS's ET-HOME EOS programme. Numerical simulations were performed on Arizona State University's Saguaro cluster, operated by ASU Research Computing. We thank two anonymous reviewers who provided many helpful suggestions.

Appendix A. Supplementary material

Supplementary material related to this article can be found online at https://doi.org/10.1016/j.epsl.2018.08.055.

References

Armann, M., Tackley, P.J., 2012. Simulating the thermochemical magmatic and tectonic evolution of Venus's mantle and lithosphere: two-dimensional models. J. Geophys. Res. 117, E12003.
Aubert, J., Labrosse, S., Poitou, C., 2009. Modelling the palaeo-evolution of the geodynamo. Geophys. J. Int. 179, 1414–1428.
Badro, J., Siebert, J., Nimmo, F., 2016. An early geodynamo driven by exsolution of mantle components from Earth's core. Nature 536, 326–328.
Bjonnes, E., Hansen, V., James, B., Swenson, J., 2012. Equilibrium resurfacing of Venus: results from new Monte Carlo modeling and implications for Venus surface histories. Icarus 217, 451–461.
Blanchard, I., Siebert, J., Borensztajn, S., Badro, J., 2017. The solubility of heat-producing elements in Earth's core. Geochem. Perspect. Lett., 1–5.
Chidester, B.A., Rahman, Z., Righter, K., Campbell, A.J., 2017. Metal–silicate partitioning of U: implications for the heat budget of the core and evidence for reduced U in the mantle. Geochim. Cosmochim. Acta 199, 1–12.
Driscoll, P., Bercovici, D., 2013. Divergent evolution of Earth and Venus: influence of degassing, tectonics, and magnetic fields. Icarus 226, 1447–1464.
Driscoll, P., Bercovici, D., 2014. On the thermal and magnetic histories of Earth and Venus: influences of melting, radioactivity, and conductivity. Phys. Earth Planet. Inter. 236, 36–51.
Du, Z., Jackson, C., Bennett, N., Driscoll, P., Deng, J., Lee, K.K., Greenberg, E., Prakapenka, V.B., Fei, Y., 2017. Insufficient energy from MgO exsolution to power early geodynamo. Geophys. Res. Lett. 44, 11,376–11,381.
Dumoulin, C., Tobie, G., Verhoeven, O., Rosenblatt, P., Rambaux, N., 2017. Tidal constraints on the interior of Venus. J. Geophys. Res., Planets 122, 1338–1352.
Elkins-Tanton, L.T., Smrekar, S.E., Hess, P.C., Parmentier, E.M., 2007. Volcanism and volatile recycling on a one-plate planet: applications to Venus. J. Geophys. Res. 112, E04S06.
Foley, B.J., Driscoll, P.E., 2016. Whole planet coupling between climate, mantle, and core: implications for rocky planet evolution. Geochem. Geophys. Geosyst. 17, 1885–1914.
Gaillard, F., Scaillet, B., 2014. A theoretical framework for volcanic degassing chemistry in a comparative planetology perspective and implications for planetary atmospheres. Earth Planet. Sci. Lett. 403, 307–316.
Gillmann, C., Chassefière, E., Lognonné, P., 2009. A consistent picture of early hydrodynamic escape of Venus atmosphere explaining present Ne and Ar isotopic ratios and low oxygen atmospheric content. Earth Planet. Sci. Lett. 286, 503–513.
Gillmann, C., Golabek, G.J., Tackley, P.J., 2016. Effect of a single large impact on the coupled atmosphere–interior evolution of Venus. Icarus 268, 295–312.
Gillmann, C., Tackley, P., 2014. Atmosphere/mantle coupling and feedbacks on Venus. J. Geophys. Res., Planets 119, 1189–1217.
Gilmore, M., Treiman, A., Helbert, J., Smrekar, S., 2017. Venus surface composition constrained by observation and experiment. Space Sci. Rev. 212, 1511–1540.
Gomi, H., Ohta, K., Hirose, K., Labrosse, S., Caracas, R., Verstraete, M.J., Hernlund, J.W., 2013. The high conductivity of iron and thermal evolution of the Earth's core. Phys. Earth Planet. Inter. 224, 88–103.
Guest, J., Stofan, E.R., 1999. A new view of the stratigraphic history of Venus. Icarus 139, 55–66.
Herrick, R.R., Rumpf, M.E., 2011. Postimpact modification by volcanic or tectonic processes as the rule, not the exception, for Venusian craters. J. Geophys. Res. 116, E02004.
Hirose, K., Labrosse, S., Hernlund, J., 2013. Composition and state of the core. Annu. Rev. Earth Planet. Sci. 41, 657–691.
Hirose, K., Morard, G., Sinmyo, R., Umemoto, K., Hernlund, J., Helffrich, G., Labrosse, S., 2017. Crystallization of silicon dioxide and compositional evolution of the Earth's core. Nature 543, 99–102.

Hirose, K., Takafuji, N., Sata, N., Ohishi, Y., 2005. Phase transition and density of subducted MORB crust in the lower mantle. Earth Planet. Sci. Lett. 237, 239–251.
Jacobson, S.A., Rubie, D.C., Hernlund, J., Morbidelli, A., Nakajima, M., 2017. Formation, stratification, and mixing of the cores of Earth and Venus. Earth Planet. Sci. Lett. 474, 375–386.
de Koker, N., Steinle-Neumann, G., Vlcek, V., 2012. Electrical resistivity and thermal conductivity of liquid Fe alloys at high P and T, and heat flux in Earth's core. Proc. Natl. Acad. Sci. USA 109, 4070–4073.
Konôpková, Z., McWilliams, R.S., Gómez-Pérez, N., Goncharov, A.F., 2016. Direct measurement of thermal conductivity in solid iron at planetary core conditions. Nature 534, 99–101.
Konopliv, A.S., Yoder, C.F., 1996. Venusian k2 tidal love number from Magellan and PVO tracking data. Geophys. Res. Lett. 23, 1857–1860.
Labrosse, S., 2015. Thermal evolution of the core with a high thermal conductivity. Phys. Earth Planet. Inter. 247, 36–55.
Landeau, M., Aubert, J., Olson, P., 2017. The signature of inner-core nucleation on the geodynamo. Earth Planet. Sci. Lett. 465, 193–204.
Lay, T., Hernlund, J., Buffett, B.A., 2008. Core–mantle boundary heat flow. Nat. Geosci. 1, 25–32.
McKinnon, W.B., Zhanle, K.J., Ivanov, B.D., Melosh, J.H., 1997. Cratering on Venus: models and observations. In: Venus II. Arizona Univ. Press, pp. 969–1014.
Nakagawa, T., Tackley, P.J., 2010. Influence of initial CMB temperature and other parameters on the thermal evolution of Earth's core resulting from thermochemical spherical mantle convection. Geochem. Geophys. Geosyst. 11.
Nakagawa, T., Tackley, P.J., 2014. Influence of combined primordial layering and recycled MORB on the coupled thermal evolution of Earth's mantle and core. Geochem. Geophys. Geosyst. 15, 619–633.
Nakagawa, T., Tackley, P.J., 2015. Influence of plate tectonic mode on the coupled thermochemical evolution of Earth's mantle and core. Geochem. Geophys. Geosyst. 16, 3400–3413.
Nimmo, F., 2002. Why does Venus lack a magnetic field? Geology 30, 987.
Noack, L., Breuer, D., Spohn, T., 2012. Coupling the atmosphere with interior dynamics: implications for the resurfacing of Venus. Icarus 217, 484–498.
Ohta, K., Hirose, K., Lay, T., Sata, N., Ohishi, Y., 2008. Phase transitions in pyrolite and MORB at lowermost mantle conditions: implications for a MORB-rich pile above the core–mantle boundary. Earth Planet. Sci. Lett. 267, 107–117.
Ohta, K., Kuwayama, Y., Hirose, K., Shimizu, K., Ohishi, Y., 2016. Experimental determination of the electrical resistivity of iron at Earth's core conditions. Nature 534, 95–98.
O'Rourke, J.G., Korenaga, J., 2015. Thermal evolution of Venus with argon degassing. Icarus 260, 128–140.
O'Rourke, J.G., Korenaga, J., Stevenson, D.J., 2017. Thermal evolution of Earth with magnesium precipitation in the core. Earth Planet. Sci. Lett. 458, 263–272.
O'Rourke, J.G., Smrekar, S.E., 2018. Signatures of lithospheric flexure and elevated heat flow in stereo topography at coronae on Venus. J. Geophys. Res., Planets 123, 369–389.
O'Rourke, J.G., Stevenson, D.J., 2016. Powering Earth's dynamo with magnesium precipitation from the core. Nature 529, 387–389.
O'Rourke, J.G., Wolf, A.S., Ehlmann, B.L., 2014. Venus: interpreting the spatial distribution of volcanically modified craters. Geophys. Res. Lett. 41, 8252–8260.
Phillips, J.L., Russell, C.T., 1987. Upper limit on the intrinsic magnetic field of Venus. J. Geophys. Res. 92, 2253.
Phillips, R.J., Bullock, M.A., Hauck, S.A., 2001. Climate and interior coupled evolution on Venus. Geophys. Res. Lett. 28, 1779–1782.
Pozzo, M., Davies, C., Gubbins, D., Alfè, D., 2012. Thermal and electrical conductivity of iron at Earth's core conditions. Nature 485, 355–358.
Seagle, C.T., Cottrell, E., Fei, Y., Hummer, D.R., Prakapenka, V.B., 2013. Electrical and thermal transport properties of iron and iron-silicon alloy at high pressure. Geophys. Res. Lett. 40, 5377–5381.
Smirnov, A.V., Tarduno, J.A., Kulakov, E.V., McEnroe, S.A., Bono, R.K., 2016. Palaeointensity, core thermal conductivity and the unknown age of the inner core. Geophys. J. Int. 205, 1190–1195.
Smrekar, S.E., Sotin, C., 2012. Constraints on mantle plumes on Venus: implications for volatile history. Icarus 217, 510–523.
Solomatov, V.S., Moresi, L.N., 1996. Stagnant lid convection on Venus. J. Geophys. Res. 101, 4737–4753.
Stacey, F., Loper, D., 2007. A revised estimate of the conductivity of iron alloy at high pressure and implications for the core energy balance. Phys. Earth Planet. Inter. 161, 13–18.
Stelzer, Z., Jackson, A., 2013. Extracting scaling laws from numerical dynamo models. Geophys. J. Int. 193, 1265–1276.
Stevenson, D.J., 2003. Planetary magnetic fields. Earth Planet. Sci. Lett. 208, 1–11.
Stevenson, D.J., Spohn, T., Schubert, G., 1983. Magnetism and thermal evolution of the terrestrial planets. Icarus 54, 466–489.
Strom, R., Schaber, G., Dawson, D., 1994. The global resurfacing of Venus. J. Geophys. Res. 99, 10899–10926.
Tarduno, J.A., Blackman, E.G., Mamajek, E.E., 2014. Detecting the oldest geodynamo and attendant shielding from the solar wind: implications for habitability. Phys. Earth Planet. Inter. 233, 68–87.
Tarduno, J.A., Cottrell, R.D., Watkeys, M.K., Hofmann, A., Doubrovine, P.V., Mamajek, E.E., Liu, D., Sibeck, D.G., Neukirch, L.P., Usui, Y., 2010. Geodynamo, solar wind, and magnetopause 3.4 to 3.45 billion years ago. Science 327, 1238–1240.
Way, M.J., Del Genio, A.D., Kiang, N.Y., Sohl, L.E., Grinspoon, D.H., Aleinov, I., Kelley, M., Clune, T., 2016. Was Venus the first habitable world of our solar system? Geophys. Res. Lett. 43, 8376–8383.
Wichman, R.W., 1999. Internal crater modification on Venus: recognizing crater-centered volcanism by changes in floor morphometry and floor brightness. J. Geophys. Res. 104, 21957–21977.
Xie, S., Tackley, P.J., 2004. Evolution of helium and argon isotopes in a convecting mantle. Phys. Earth Planet. Inter. 146, 417–439.